Electronic Supplementary Material (ESI) for Journal of Analytical Atomic Spectrometry.
This journal is © The Royal Society of Chemistry 2022

Supplementary Material

Tuning and Acquisition parameters selection

Choice of ICPMS sampling depth:
ICPMS sampling depth is defined as the distance between the torch and the sample cone. The choice of sampling depth is based on optimization of sensitivity without compromising the accuracy or precision of $\delta^{11}B$ determination. This optimization was done at five different sampling depths: (i) 3.5mm, (ii) 4.5mm, (iii) 5mm (iv) 5.5mm and (v) 6.5 mm (Figure S4). Higher sampling depths were not explored in detail due to severe (~50%) loss in sensitivity. We analyzed SRM AE-121 against NIST 951a at the same concentration under identical tuning conditions at these five sampling depths. During the change in sampling depth instrument sensitivity was optimized by tuning for the torch position (x- and y-axis), sample- and additional-gas flow while maintaining the rest of the tuning parameters and detection settings constant. The key observations were: both sensitivity and mass bias decreased with increasing sampling depth (Figure S4A, S4B); and a comparable accuracy was obtained for all sampling depths below 5mm (~19.65‰). However, the best precision is obtained at sampling depths of 4.5mm. Thus, for all the further analyses instrument was optimized at the sampling depth of 4.5mm (figure S4C). The choice of sampling depth plays a critical role in determining both sensitivity and the mass bias. Mass bias can be defined as the deviation of measured $^{11}B/^{10}B$ ratio from the true value. In theory, plasma sampling depth should have minimal to no impact on the accuracy or the precision of the isotope analyses. However, we observe that at short a sampling depth (3.5mm), the mass bias is high and as the sampling depth increases the mass bias decreases (Figure S4). This observation may be explained through the plasma space charge effect. In an Argon plasma, $^{40}Ar^{+}$ dominates, and there is strong ion-ion repulsion between the analyte cation and the argon ion. The impact of these repulsions is more severe for light masses than heavier masses. For boron there is about 10% mass difference between the ^{10}B and ^{11}B and thus the repulsion driven radially outward scattering for the lighter isotope(^{10}B) is relatively larger than for the heavier isotope (^{11}B). As a result, at a short sampling depth less ^{10}B is sampled resulting in higher mass bias. Thus, the observed mass bias for the light masses is higher than the true ratio.

Quadrupole Scanning Mode: The QQQ-ICP-MS offers two possible modes of acquisition (a) spectrum mode and (b) peak profile mode. In spectrum mode the quadrupole mass filter operates by scanning with a unit mass resolution. Whereas in peak profile mode the mass spectra are obtained by scanning Q1 and Q2 between 1 and 20 points/mass. The choice of the quadrupole scanning mode, spectrum vs. MS/MS, has a strong impact on the final sensitivity and analyses time. Thus, their impact on $\delta^{11}B$ accuracy and precision was evaluated through repeat analyses of NIST 951a at a constant boron concentration of 8 ppb. All of the tuning parameters were held constant during these experiments, only the mode of quadrupole scanning was changed from spectrum to MS/MS. We measured $^{11}B/^{10}B$ ratio in three possible modes, Spectrum Single Quad, Spectrum MS/MS, Peak profile mode, while keeping the number of replicates/sweeps fixed. Between spectrum single quad mode and peak profile (MS/MS) mode we observe a comparable accuracy and precision. The spectrum single quad mode had a higher number of ion counts, and a lower sample analyses time (for a set number of replicates/sweeps). Thus, all the further analyses were performed in the spectrum single quad mode (Figure S7).

Ion Detection Mode: The secondary electron multiplier of the instrument offers two modes for ion detection – (a) Pulse mode (≤ 0.7 – 1Mcps) and (b) Analog mode (≥ 0.7 Mcps). For accurate and precise isotope ratio determination both isotopes should be determined in the same ion detection mode. We evaluated the impact of the choice of detection mode (pulse vs. analog) on the accuracy and precision of $\delta^{11}B$ determination. Under identical tuning conditions and boron concentration, SRM AE-120 was analyzed (n = 3) following the SSB technique in the two different detection modes. Both isotopes were determined in the same mode (pulse-pulse or analog-analog). The ^{11}B sensitivity was ~0.5 Mcps to ensure a minimum of 100,000 counts on ^{10}B. Both detection modes have identical accuracy; however, we observed a higher precision in pulse mode (-20.31 ± 0.05‰, 2σ) over analog mode (-18.82 ± 3.8‰, 2 σ) (figure S8). Thus, all boron isotopic measurements were done exclusively in pulse mode.

Resolution Mode: The Agilent™ 8900 offers ion detection in either in standard resolution (M/ΔM = 1 amu) or at a narrow resolution (M/ΔM = 0.5 amu) for the acquisition of the signal. The impact of the choice of the resolution mode on accuracy and precision was evaluated through analyses of NIST 951a. We kept all the tuning parameters constant during these experiments. Only the resolution mode of detection was switched from standard to narrow resolution. We observe a higher precision in standard resolution mode over narrow resolution mode (Figure S9).

Choice of Replicates and Sweeps
During an individual analyses mass spectrometric ion counting is divided into replicates and sweeps. Specified number of sweeps make a single replicate. Ideally the choice of replicates and sweeps should only impact the precision based on total duration of acquisition (counting statistics). The effect of each of these parameters on the accuracy and precision of $\delta^{11}B$ measurements were studied in detail. At an equivalent number of replicates and

sweeps, we observe a high precision. Thus, a combination of replicates and sweeps ranging from 50/50 to 100/100 were evaluated. Since the choice of replicates/sweeps determines the total acquisition time, our aim was to optimize precision at the least possible acquisition time.

The key observations from these experiments are: (i) For both low replicates and high sweeps and high replicates and low sweeps, we have poor precision (> 3‰, 2σ). (ii) At equivalent replicates and sweeps high precision is observed. Thus, as expected the accuracy of $d^{11}B$ determination was independent of the choice of combination of Replicates/Sweeps, however the precision is strongly dependent on the ratio of replicates to sweeps. A possible explanation for the observed lower precision at high replicates and low sweeps could be due to low acquisition time for each replicate where short term high frequency instrumental drift leads to lower precision. Since the averaging is done over a short period of time any fluctuation in sensitivity due to plasma flicker and instrumental drift are not averaged out. Increasing number of sweeps results in an unusually high acquisition time at a single replicate and possibly leads to detector saturation and resulting in lower precision. At an equivalent number of replicates and sweeps, we observe a high precision. Thus, it was further investigated in further details by varying the combination of replicates and sweeps from 50/50 to 100/100. We performed triplicate measurements of NIST 951a at nine different combinations of Replicates/Sweeps while keeping all other tuning parameters constant. Replicates and sweeps were varied between 50 replicates to 100 replicates and between 50 sweeps to 100 sweeps in units of 25. Minimum acquisition time was 65.514s for a replicates/sweeps = 50/50 and 150.02s for replicates/sweeps = 100/100 (Figure S6B). Thus, there was a 150% increase in acquisition time over the course of the experiment. Please refer to Table – S1 for the selected combination of replicates/sweeps and their corresponding acquisition times. We observe that with an increase in acquisition time the mass bias increases. Both replicates and sweeps independently impacts mass bias. Despite this increase in mass bias neither the accuracy nor the precision of the $d^{11}B$ determination is compromised. A possible reason for the increase in mass bias is due to the impact on detector dead time due to variation in the acquisition time. The detector dead time is the minimum amount of time required between two consecutive ion impact detections.

Figure S1: Speciation of Boron in natural waters.

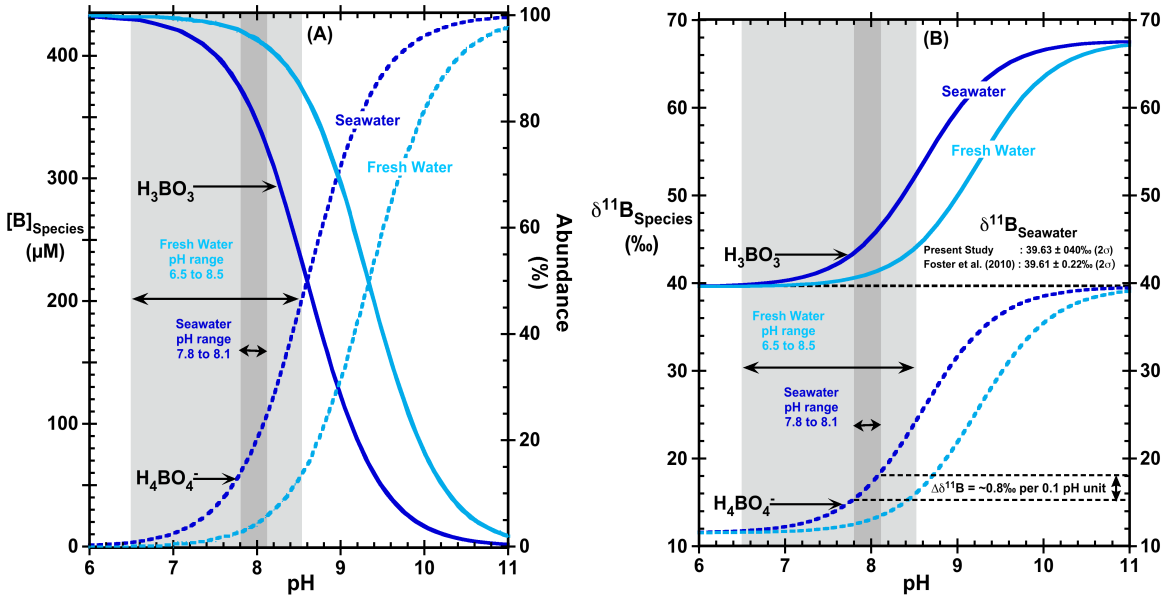

Figure. S1: Calculated speciation of boron (boric acid vs. borate ion) (Panel A) and the isotopic composition ($\delta^{11}B$) of each species (Panel B) as a function of solution pH (T = 25°C). The calculations for freshwater (S = 0 psu) and for seawater (S = 35 psu) are represented by light blue and dark blue lines respectively.

Figure S2: Impact of ICP-MS acid matrix on the Boron Washout time

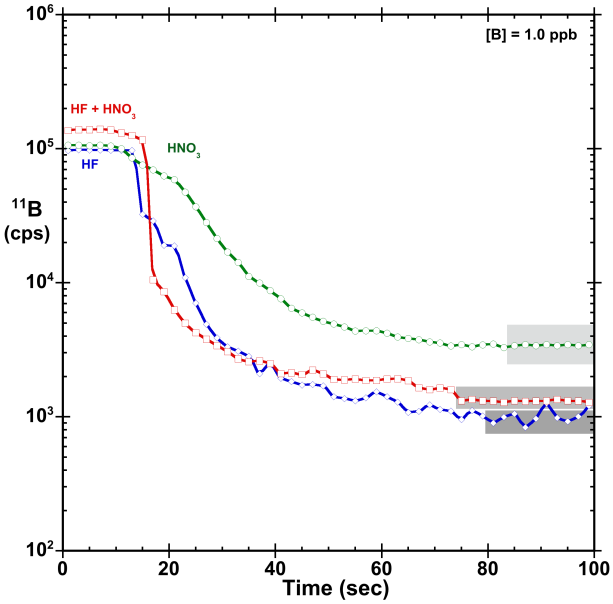

Figure. S2: Determination of boron washout time in 2% nitric acid (green circles), 0.3M HF (blue diamonds), and 0.3M HF + 0.1M HNO_3 (red squares) matrix. Analyses were done by alternating between a 1 ppb boron solution and the acid blank of the same exact matrix. ^{11}B counts are plotted in logarithmic scale on the Y- axis against the time (s) on the X-axis. The grey bar represents the section of identical blank values obtained prior to the introduction of 1ppb B solution to the spray chamber.

Figure S3: Impact of Spray Chamber temperature on Boron sensitivity.

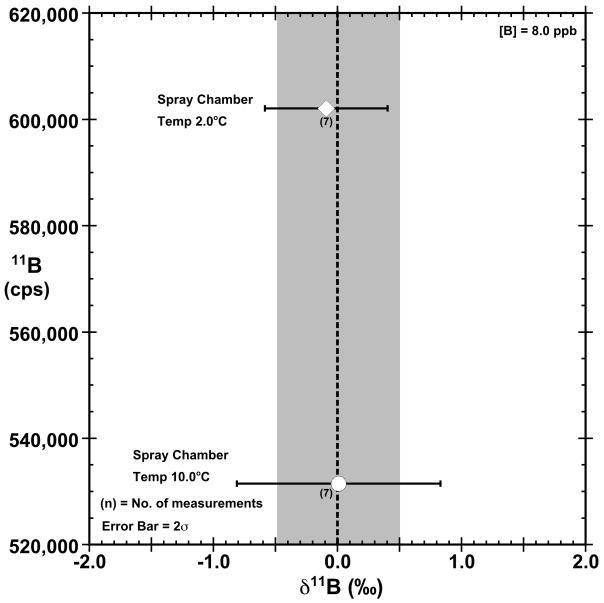

Figure. S3: The impact of spray chamber temperature on boron sensitivity and δ^{11}B accuracy and precession. Boron sensitivity (Y-axis) is plotted against the δ^{11}B (X-axis). The tuning parameters were kept constant, and the spray chamber temperature was varied from 2°C (diamond) to 10°C (circle). Each data point represents an average of seven δ^{11}B values based on 9 consecutive NIST ^{11}B/^{10}B determinations. The error bars represent the 2σ analytical uncertainty. The dashed line represents the value of NIST 951a (0.0‰), and the grey bar represents a ± 0.5‰ window of uncertainty.

Figure S4: Effect of sampling depth on Boron sensitivity, Mass Bias and $\delta^{11}B$.

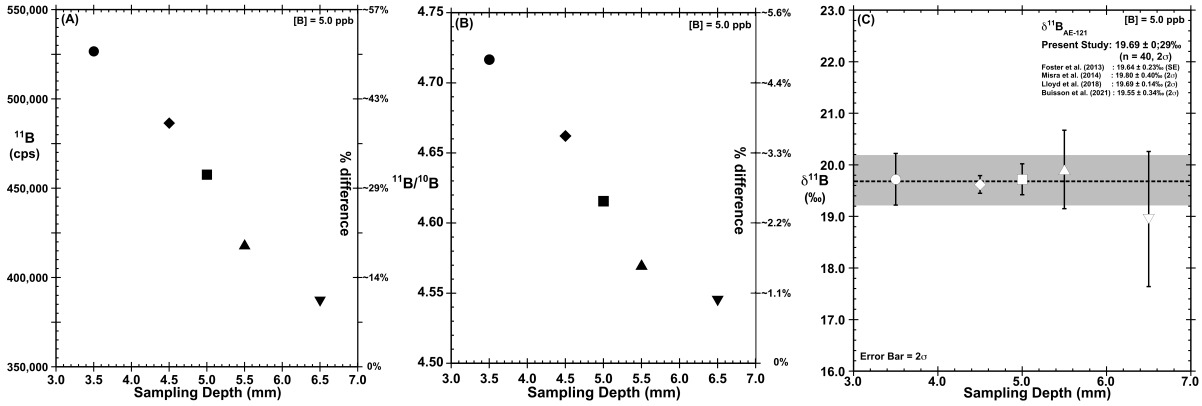

Figure. S4: Impact of plasma sampling depth on Boron sensitivity (Panel A), Mass Bias (Panel B) and, δ^{11}B (panel C). Primary Y-axis (LHS) represents the ^{11}B sensitivity (Panel A); mass bias (panel B), and δ^{11}B (panel C). In panels A and B, the percentage (%) change in sensitivity is shown on the secondary Y-axis (RHS). All analyses were performed on NIST 951a standard at 5 ppb boron concentration during the same instrumental session. The analyses were conducted at sampling depths (i.e., torch position) of 3.5mm (circle), 4.5mm (diamond), 5mm (square), 5.5mm (triangle), and 6.5mm (down triangle) from the sampling cone. At each sampling depth, sensitivity was optimized by tuning for sample gas, makeup gas and torch position (horizontal and vertical position). The rest of the tuning parameters were kept constant. Each data point represents the average of triplicate measurements acquired during a single instrument session bracketed by NIST 951. In panel C The dashed line and the grey bar represents the published value of AE -121 (19.69‰) and a ± 0.5‰ window of uncertainty respectively.

Figure S5: Effect of Integration time on $\delta^{11}B$ Boron accuracy and precision.

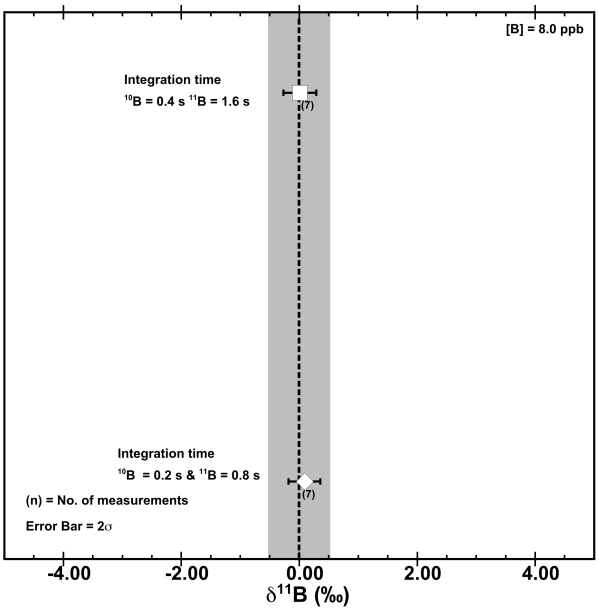

Figure. S5: The effect of ion beam integration time on the $\delta^{11}B$ accuracy and precession. The integration time was varied in the inverse ratio of the natural abundance of the two boron isotopes. We explored two different combinations of integration time (i)0.2s, 0.8s (ii)0.4s, 1.6s on ^{10}B and ^{11}B respectively. The open diamond represents the integration time of ^{10}B and ^{11}B as 0.2s &0.8s, and the open square represents the integration time of ^{10}B and ^{11}B as 0.4s &1.6s. All analyses were done at 8 ppb boron concentration under identical tuning conditions. Each data point represents an average of seven $\delta^{11}B$ values based on 9 consecutive NIST $^{11}B/^{10}B$ determinations. The error bar represents 2σ analytical uncertainty. The dashed line represents the value of NIST 951a (0.0‰), and the grey bar represents a ± 0.5‰ window of uncertainty.

Figure S6: Impact of combination of replicates/sweeps on $\delta^{11}B$ Boron accuracy and precision.

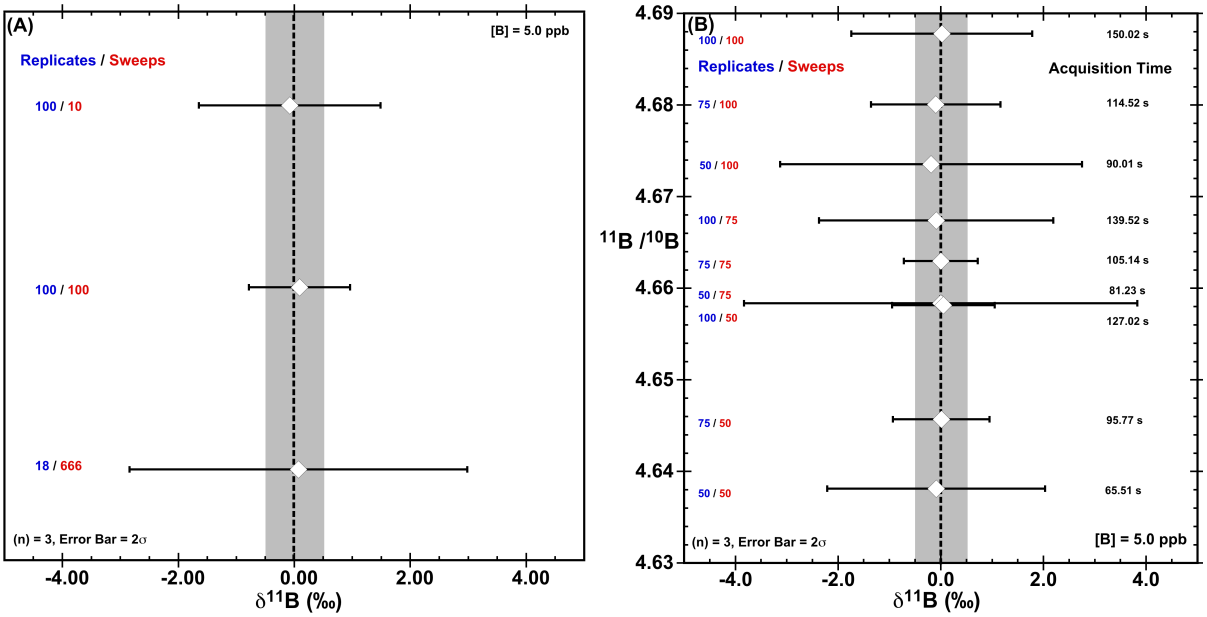

Figure. S6: Variations in accuracy and precession of $\delta^{11}B_{NIST\text{-}951a}$ determination as a function of choice of replicates and sweeps. In panel A: the $\delta^{11}B$ values (X-axis) are sorted according to an increasing number of sweeps (Y-axis). In panel B: the $\delta^{11}B$ (X-axis) is plotted against increasing mass bias (Y-axis). All analyses were performed under identical tuning conditions with a constant boron concentration of 3.5 ppb. In panels A and B, the combination of replicates and sweeps are tabulated on LHS, and their corresponding total acquisition times are tabulated on the RHS. Each data point represents an average of seven $\delta^{11}B$ values based on 9 consecutive NIST $^{11}B/^{10}B$ determinations. The error bar represents 2σ analytical uncertainty. The dashed line and the grey bar represent the $\delta^{11}B$ value of NIST 951a (0.0‰) and a ± 0.5‰ window of uncertainty respectively.

Figure S7: Impact of different acquisition mode on $\delta^{11}B$ Boron accuracy and precision.

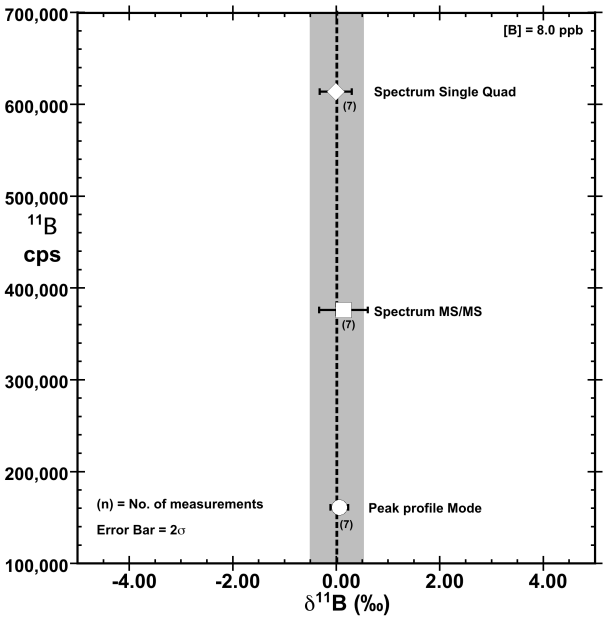

Figure. S7: The impact of the choice of peak scanning modes (i) peak profile mode (open circle), (ii) Spectrum MS/MS mode (open square), (iii) spectrum single Quad mode (open diamond) on boron sensitivity as well as $\delta^{11}B$ accuracy and precession. ^{11}B sensitivity (Y-axis) is plotted against the $\delta^{11}B$ (X-axis). All analyses were done at a constant B concentration of 8 ppb under identical tuning conditions. Each data point represents average of seven $\delta^{11}B$ values based on 9 consecutive NIST $^{11}B/^{10}B$ determinations. The error bars represent the 2σ analytical uncertainty. The dashed line represents the value of NIST 951a (0.0‰), and the grey bar represents a ± 0.5‰ window of uncertainty.

Figure S8: Effect of detection mode on $\delta^{11}B$ Boron accuracy and precision.

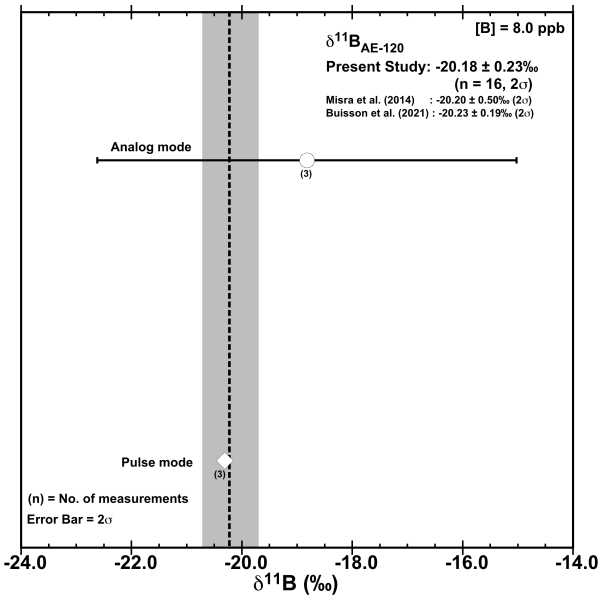

Figure. S8: The accuracy and precession of $\delta^{11}B_{AE\text{-}120}$ determination in pulse (open diamond) vs. analog (open circle) ion detection mode. Both isotopes of boron were measured in the same ion detection mode. Determination in both modes were done following SSB protocol at 8 ppb boron concentration. Each data point represents the average of triplicate analyses. All analyses were performed during a single instrument session under identical tuning conditions. Only the ion detection mode (analog/pulse) was changed during the analyses. The average $\delta^{11}B$ for pulse mode is –20.31±0.05‰, 2σ and for analog mode is –18.82±3.8‰, 2σ. The error bar represents 2σ analytical uncertainty. The dashed line represents the accepted value of SRM AE-120 (-20.2‰), and the grey bar represents a ± 0.5‰ window of uncertainty.

Figure S9: Effect of resolution mode on $\delta^{11}B$ Boron accuracy and precision.

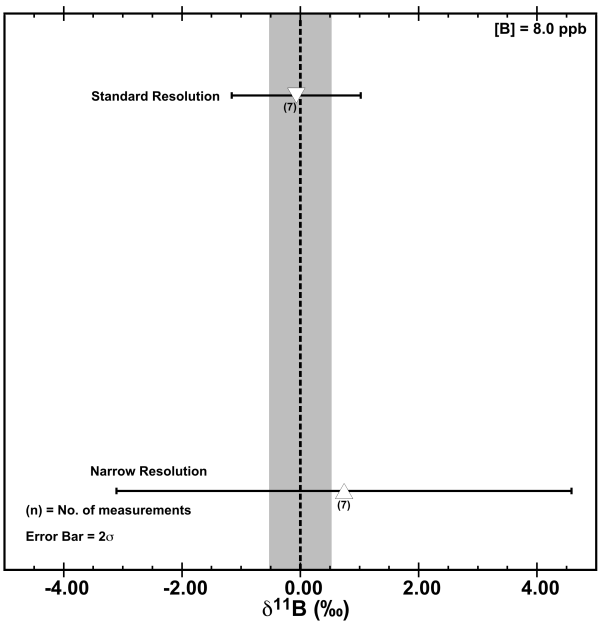

Figure. S9: The impact of the peak scanning resolution (standard vs. narrow) on $\delta^{11}B_{NIST\text{-}951}$ accuracy and precession. Determination in both modes were done following SSB protocol at 8 ppb boron concentration. Each data point represents an average of seven $\delta^{11}B$ values based on 9 consecutive NIST $^{11}B/^{10}B$ determinations. All analyses were performed during a single instrument session under identical tuning conditions under pulse detection mode by changing the resolution mode from standard resolution (down triangle) to narrow resolution (up triangle). The average $\delta^{11}B$ for standard resolution mode is –0.07±1.0‰, 2σ and for narrow resolution mode is 0.74±3.8‰, 2σ. The error bar represents 2σ analytical uncertainty. The dashed line represents the accepted value of NIST 951a (0.0‰), and the grey bar represents a ± 0.5‰ window of uncertainty.

Figure S10: Temporal drift in Instrumental mass bias with time.

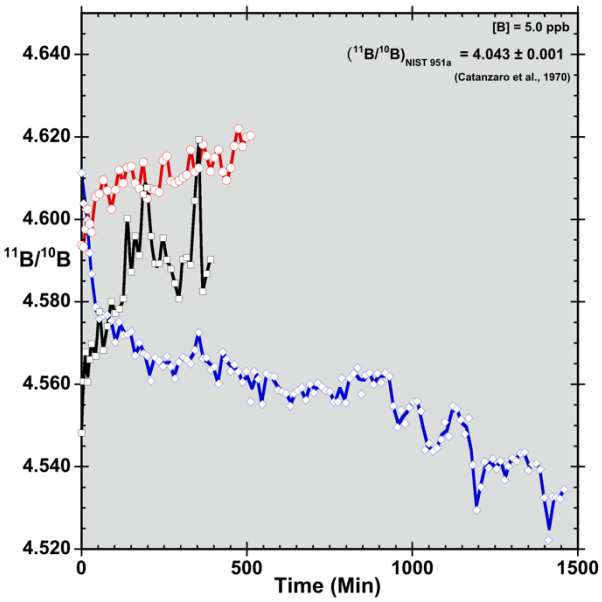

Figure. S10: Temporal drift in instrumental mass bias ($^{11}B/^{10}B$) based on repeat measurement of NIST 951a (bracketing standard) for three analytical sessions of different lengths. The mass bias is plotted on Y-axis against the section duration (in minutes) on the X-axis. The blue diamonds represent the longest run of 18 hours, whereas the black squares and red circles represent a typical run of 9-10 hours adopted in this study. The true isotope ratio of NIST-951a = 4.034 ± 0.001 is off the axis.

Table – S1 Acquisition time for the corresponding choice of replicate and sweeps.

Replicates	Sweeps	Acquisition time (seconds)
50	50	65.51
50	75	81.23
50	100	90.01
75	50	95.77
75	75	105.14
75	100	114.52
100	50	127.02
100	75	139.52
100	100	150.02

Table – S2 Long-term reproducibility of $\delta^{11}B$ for boric acid standard reference material AE-121

Serial Number	Date	$\delta^{11}B$-Avg	2σ	2SE	n	[B](ng/g)
1	31/03/21	19.69	0.24	0.09	7	4
2	03/04/21	19.69	0.35	0.20	11	3.5
3	04/07/21	19.65	0.37	0.19	4	4
4	05/07/21	19.43	0.48	0.22	5	7
5	24/08/21	19.79	1.06	0.61	3	2.5
6	27/08/21	20.01	0.52	0.36	2	5
7	16/09/21	19.83	0.47	0.27	3	5
8	18/09/21	19.51	0.49	0.24	4	3
9	19/09/21	19.90	0.28	0.16	3	5
10	20/09/21	19.77	0.30	0.17	3	5
11	21/09/21	19.68	0.50	0.19	7	5
12	22/09/21	19.63	0.72	0.29	6	5
13	23/09/21	19.75	0.57	0.18	10	5
14	21/10/21	19.63	0.44	0.18	6	7.5
15	22/10/21	19.97	0.32	0.19	3	7
16	23/10/21	19.50	0.47	0.19	6	7
17	24/10/21	19.62	0.33	0.13	6	6
18	25/10/21	19.66	0.53	0.27	4	5
19	26/10/21	19.79	0.41	0.16	7	5
20	27/10/21	19.67	0.22	0.09	6	5
21	28/10/21	19.74	0.42	0.12	12	4.5
22	29/10/21	19.75	0.58	0.22	7	6
23	30/10/21	19.81	0.65	0.25	7	5
24	31/10/21	19.69	0.53	0.15	12	4.5
25	01/11/21	19.66	0.60	0.27	5	3
26	02/11/21	19.79	0.34	0.15	5	6
27	03/11/21	19.69	0.51	0.18	8	5
28	04/11/21	19.94	0.38	0.12	10	5
29	09/11/21	19.56	0.57	0.16	12	5
30	10/11/21	19.48	0.60	0.30	4	5
31	11/11/21	19.72	0.39	0.12	11	5
32	12/11/21	19.66	0.44	0.26	3	2
33	13/11/21	19.63	0.55	0.17	10	5
34	14/11/21	19.64	0.49	0.20	6	2.5
35	15/11/21	19.56	0.58	0.13	20	5
36	24/12/21	19.58	0.47	0.12	15	6
37	25/12/21	19.60	0.71	0.27	7	1.5
38	26/12/21	19.63	0.52	0.16	11	5
39	27/12/21	19.67	0.57	0.19	9	5

40	28/12/21	19.81	0.40	0.11	13	5